ORIGINAL ARTICLE

JBMR®

Molecular and Cellular Mechanisms of Delayed Fracture Healing in *Mmp10* (Stromelysin 2) Knockout Mice

José Valdés-Fernández,[1] Tania López-Martínez,[1] Purificación Ripalda-Cemboráin,[1,2] Isabel A Calvo,[3] Borja Sáez,[3] Juan Antonio Romero-Torrecilla,[1] Javier Aldazabal,[4] Emma Muiños-López,[1] Verónica Montiel,[2] Josune Orbe,[5] José Antonio Rodríguez,[5] José Antonio Páramo,[5,6] Felipe Prósper,[1,3,6] and Froilán Granero-Moltó[1,2]

[1]Cell Therapy Area, Clínica Universidad de Navarra, Pamplona, Spain
[2]Department of Orthopaedic Surgery and Traumatology, Clínica Universidad de Navarra, Pamplona, Spain
[3]Hematology-Oncology Program, Centro de Investigación Médica Aplicada (CIMA), Instituto de Investigación Sanitaria de Navarra (IdiSNA), Pamplona, Spain
[4]Tissue Engineering Group, TECNUN-Universidad de Navarra, San Sebastián, Spain
[5]Atherotrombosis, Cardiovascular Disease Program, CIMA, Instituto de Investigación Sanitaria de Navarra (IdiSNA), CIBERCV, Pamplona, Spain
[6]Department of Hematology, Clínica Universidad de Navarra, Pamplona, Spain

ABSTRACT

The remodeling of the extracellular matrix is a central function in endochondral ossification and bone homeostasis. During secondary fracture healing, vascular invasion and bone growth requires the removal of the cartilage intermediate and the coordinate action of the collagenase matrix metalloproteinase (MMP)-13, produced by hypertrophic chondrocytes, and the gelatinase MMP-9, produced by cells of hematopoietic lineage. Interfering with these MMP activities results in impaired fracture healing characterized by cartilage accumulation and delayed vascularization. MMP-10, Stromelysin 2, a matrix metalloproteinase with high homology to MMP-3 (Stromelysin 1), presents a wide range of putative substrates identified in vitro, but its targets and functions in vivo and especially during fracture healing and bone homeostasis are not well defined. Here, we investigated the role of MMP-10 through bone regeneration in C57BL/6 mice. During secondary fracture healing, MMP-10 is expressed by hematopoietic cells and its maximum expression peak is associated with cartilage resorption at 14 days post fracture (dpf). In accordance with this expression pattern, when *Mmp10* is globally silenced, we observed an impaired fracture-healing phenotype at 14 dpf, characterized by delayed cartilage resorption and TRAP-positive cell accumulation. This phenotype can be rescued by a non-competitive transplant of wild-type bone marrow, indicating that MMP-10 functions are required only in cells of hematopoietic linage. In addition, we found that this phenotype is a consequence of reduced gelatinase activity and the lack of proMMP-9 processing in macrophages. Our data provide evidence of the in vivo function of MMP-10 during endochondral ossification and defines the macrophages as the lead cell population in cartilage removal and vascular invasion. © 2021 The Authors. *Journal of Bone and Mineral Research* published by Wiley Periodicals LLC on behalf of American Society for Bone and Mineral Research (ASBMR).

KEY WORDS: BONE FRACTURE; ENDOCHONDRAL OSSIFICATION; EXTRACELLULAR MATRIX; MACROPHAGES; MMP-10

Introduction

Unlike most tissues, after a severe injury, bone tissue develops a strong healing response. Through this healing process, bone is able to recover its original structure and functionality without forming a scar tissue. Bone healing recapitulates certain aspects of the skeletal development and growth, involving a complex interplay between cells, extracellular matrix, and growth factors. Non-stabilized bone fractures that take place in the appendicular skeleton heal by both intramembranous and endochondral ossification. The endochondral ossification process predominates in the mechanically unstable regions close to the fracture site. On the other hand, the intramembranous ossification process takes place at the proximal and distal edges of the callus, where a greater mechanical stability exists.[1-3]

In all cases, bone fracture healing implies a total remodeling of the extracellular matrix (ECM), which implies the proteolytic

Received in original form November 23, 2020; revised form June 15, 2021; accepted June 20, 2021.
Address correspondence to: Froilán Granero-Moltó, PhD, Clínica Universidad de Navarra, 36 Pío XII Avenue, 31008 Pamplona, Spain. E-mail: fgranero@unav.es
Additional Supporting Information may be found in the online version of this article.
Journal of Bone and Mineral Research, Vol. 00, No. 00, Month 2021, pp 1–11.
DOI: 10.1002/jbmr.4403

degradation of structural matrix and the deposition of new matrix proteins. Matrix metalloproteinases (MMPs) comprise a family of zinc-dependent proteases with more than 20 members. This group of enzymes is able to degrade all ECM components, having a leading role in ECM remodeling.[3-7]

The role of various MMPs during the fracture healing process has been previously studied. *Mmp2* is expressed since day 3 of the reparative process along fracture callus; *Mmp2* knockout mice show a delayed bone remodeling, as well as an altered expression pattern of other *Mmps*.[8] *Mmp9* is expressed in inflammatory cells and mesenchymal stem cells during the inflammatory phase, whereas it is expressed in osteoclasts during fracture callus remodeling phase. MMP-9 participates in soft callus remodeling and vascular invasion of the cartilage, and *Mmp9* knockout mice show cartilage accumulation at 14 days post fracture.[9] *Mmp13* is mainly expressed in hypertrophic chondrocytes and osteoblasts. MMP-13 also participates in cartilaginous callus remodeling and vascular invasion.[10,11] Despite the roles these MMPs play in fracture repair, all phenotypes displayed by the deficiency of a matrix metalloproteinase are transient, and the transgenic mice achieve a total fracture repair.

MMP-10 (Stromelysin 2) presents high homology with MMP-3 (Stromelysin 1), having a broad substrate specificity. MMP-10 is able to cleave in vitro collagens of types III, V, VII, X and XIV, laminin, and fibronectin.[12] Different studies confirm the role of MMP-10 in several biological and pathological processes. MMP-10 profibrinolytic role after blood clot has been previously reported; even more, exogenous MMP-10 supplementation has been proven as a useful tool to reduce infarct size in a murine stroke model.[13] Matrix metalloproteinase-mediated degradation of the ECM is a major factor for tumor development and expansion. Reports suggest that MMP-10 is expressed and active at high levels in human non-small-cell lung carcinoma when compared with healthy lung tissues, being a potential target for the development of new therapies in lung cancer.[14] The role of MMP-10 has also been studied in liver wound healing and regeneration, after mouse liver injury *Mmp10* expression is induced, participating in the hepatic wound healing response. In this model, silencing *Mmp10* resulted in impaired resolution of necrotic areas, increased fibrogenesis, and defective turnover of fibrin and fibronectin.[15]

MMP-10 expression in skeletal development has been previously reported. MMP-10 is expressed by osteoblast in bone formation sites as well as in chondrocytes of growth plate in human neonatal ribs.[16] The role of MMP-10 in fibrosis ossificans progressive (FOP) has been determined in vitro, and myoblast cells expressing the constitutive activated mutant ALK2 showed overexpression of *Mmp10*. Additionally, MMP-10 could enhance the differentiation of these myoblast cells into osteoblast, suggesting that MMP-10 may play a role in the heterotopic bone formation observed in FOP patients.[17] MMP-10 has also been proven to perform a leading role in macrophage migration in 2D and 3D in vitro platforms as well as macrophage activation.[18,19] This could be important because during fracture repair, macrophage migration and differentiation into osteoclast are key steps in vascularization and healing progression.

Here, we found that during fracture healing, loss of *Mmp10* results in a delayed repair phenotype, characterized by reduced gelatinase activity and impaired cartilage resorption. Biochemical analysis demonstrated that the observed phenotype derives from the incapacity of mononuclear cells from *Mmp10* knockout mice to process proMMP-9 and suggests a role for MMP-10 as a key factor that triggers vascularization of the cartilaginous callus through MMP-9 activation.

Materials and Methods

Animals

All animal procedures were approved by the University of Navarra Institutional Committee on Care and Use of Laboratory Animals (CEEA) and the Navarra Regional Government (CEEA # E8-16(107-15E1), E58-16(107-15E2), and E32-17(107-15E3)).

Seven- to 14-week-old female Mmp10$^{-/-}$ mice (Mmp10^{KO}, B6.129P2-MMP10^{tm1Jkmg} backcrossed into C57BL/6J background)[20] and C57BL/6J (wild type [WT]) (Harlan Ibérica, San Feliu de Codines, Spain) were used throughout this study.

For non-competitive bone marrow transplant, WT bone marrow was extracted from males and females B6.SJL-Ptprc^{a} Pepc^{b}/BoyJ (CD45.1, JAX stock #002014, The Jackson Laboratory, Bar Harbor, ME, USA).

For hematopoietic progenitors labeling, B6.Cg-Tg(Mx1-Cre) 1Cgr/J (Mx1-Cre, JAX stock #003556, The Jackson Laboratory) were crossed with B6.Cg-Gt(ROSA)26Sor$^{tm6(CAG-ZsGreen1)Hze}$/J (Ai6, JAX stock #007906, The Jackson Laboratory). Seven- to 14-week-old animals, males and females, of the resulting F1 (Mx1-CreAi6) were used.

In total, 140 mice were used in this study, C57BL/6J (WT, $n = 72$), B6.129P2-MMP10^{tm1Jkmg} (Mmp10^{KO}, $n = 62$), B6.SJL-Ptprc^{a} Pepc^{b}/BoyJ (CD45.1, $n = 2$), and F1 B6.Cg-Tg (Mx1-Cre) 1Cgr/J × B6.Cg-Gt(ROSA)26Sor$^{tm6(CAG-ZsGreen1)Hze}$/J (Mx1-Cre Ai6, $n = 4$).

Animals were housed in a barrier facility with a 24-hour light/dark cycle and feed with standard mice chow. Mice were given *ad libitum* access to food and water.

Closed fractures and surgeries

For all procedures, animals were anesthetized employing isoflurane (B. Braun Vet Care, Tuttlingen, Germany), and buprenorphine (0.05 mg/kg body weight) was injected subcutaneously for postoperative pain control.

Stabilized close fractures were produced in 7- to 14-week-old females by intramedullary fixation as described previously.[21,22] Radiographic imaging was performed to assess proper fixation and fracture.

Hematopoietic progenitors were labeled by inducing Mx-1 promoter with intraperitoneal injection of poly I:C (pI:pC, 12.5 mg/kg/d), 4 doses in alternate days. After the last pI:pC injection, animals were subjected to a non-stabilized fracture of the tibia. Non-stabilized tibia fractures were carried out using a three-point device without intramedullar fixation.

Animals were euthanized at 5, 7, 10, 14, or 21 days post fracture (dpf) employing carbon dioxide (CO_2).

For unicortical bone defects, a unicortical defect was created using a 0.8 mm drill (see Supplemental Materials and Methods for detailed procedure). Animals were euthanized at 14 and 21 dpf employing carbon dioxide (CO_2).

Micro-computed tomography (μCT) analysis

For μCT analysis, mice were euthanized, the tibias or femurs were extracted, and the pin removed. Tomographic images of the mice tibias were acquired using X-ray micro-CT (Micro-CAT II, Siemens PreClinical Solutions, Knoxville, TN, USA) with the following parameters: 80 kVp X-ray source voltage, 250 μA current, and

1250 ms exposure time per projection. Seven hundred projections were acquired with isotropic 10 μm voxel size and a resolution of 1216 × 1216 pixels. CT images were automatically reconstructed using the Cobra software (Exxim Computing Corporation, Pleasanton, CA, USA). 3D bone images were rendered using the Amira 3D Software for preclinical analysis (Thermo Fisher Scientific, Waltham, MA, USA).

Histology, immunofluorescence, and TRAP staining and quantification

After mice were euthanized, tibias were dissected, washed with PBS, and fixed for 48 hours with 4% PFA (PanReac, Barcelona, Spain). Fixated tibias were decalcified, dehydrated in graded ethanol, and embedded in paraffin as previously described.[21,23] Whole calluses of fractured tibias were serially sectioned in the sagittal plane with a HM 340 E microtome (Microm, Boise, ID, USA) at 4 μm thickness. For histological evaluation, selected sections (1 every 10 slides) were hydrated in decreasing graded ethanol and stained with Toluidine blue (TB).

For immunofluorescence analysis, sections were treated sequentially for antigen unmasking with 4 mg/mL of hyaluronidase (H-3884, Sigma-Aldrich, St. Louis, MO, USA) in PBS, pH 5.5 for 15 minutes at 37°C, and with 4 mg/mL of pepsin (P6887, Sigma-Aldrich) in HCl 0.01 N for 30 minutes at 37°C. Primary antibodies anti-type II collagen (631711, MP Biomedicals, Santa Ana, CA, USA), anti-MMP-9 (ABT544, Millipore, Burlington, MA, USA), anti-type X collagen (234196, Millipore), anti-MMP-10 (ABIN3185594, Antibodies Online, Aachen, Germany), and anti-F4/80 (ab6640, Abcam, Cambridge, UK) were employed. For F4/80 antibody, antigen unmasking was carried out with 1 mg/mL trypsin (A4148, PanReac) in PBS containing 1 mg/mL of $CaCl_2$ for 1 hour at 37°C. Secondary antibodies conjugated to fluorochrome were used (Alexa Fluor, Invitrogen, Carlsbad, CA, USA).

For the TRAP analysis, the Leukocyte Acid Phosphatase (TRAP) Kit (387A-1KT, Sigma-Aldrich) was employed. TRAP staining was performed following manufacturer instructions.

Bright-field digital images were acquired with an Aperio scan (Leica Biosystems, Nussloch, Germany). Immunofluorescent images were acquired with a Zeiss AxioCam MRm1 (Plan-Neofluar objective with 0.50 NA) with an AxioImager.M1 microscope (Carl Zeiss, Oberkochen, Germany).

Histological preparations, TRAP staining, and immunofluorescence preparations (2 to 3 central sections, $n = 3–5$) were quantified using ImageJ/Fiji software with custom macros. The signal was quantified as total area (arbitrary units).

All digital images were imported into Adobe Photoshop and formatted. Illustrations were created with Biorender.com

Bone marrow isolation and osteoclast differentiation

Osteoclastic cells were differentiated from the monocyte/macrophage lineage of the bone marrow. Bone marrow was extracted and isolated from hindlimbs of WT and $Mmp10^{KO}$ mice ($n = 6$ each) as previously reported.[24] Briefly, femurs and tibias were dissected, and bone marrow was flushed using PBS. Bone marrow cells were centrifuged at 600*g* for 8 minutes. Cell pellet was resuspended in 10 mL of fresh PBS and mononuclear cells were isolated employing 10 mL of Ficoll solution (Ficoll-Paque, GE Healthcare Bio-Sciences AB, Uppsala, Sweden) to create a density gradient. PBS/Ficoll mixture was centrifuged at 200*g* for 20 minutes to separate cells into three layers. The middle layer, which contains mononuclear cells, was gently removed and washed with PBS.

Mononuclear cells from WT and $Mmp10^{KO}$ mice were seeded in P6 plates and were cultured for 3 days with bone marrow macrophage induction media (BM-MIM), MEM Alpha Medium (Gibco, Thermo Fisher Scientific) supplemented with 10% fetal bovine serum (F7524, Sigma), 1% penicillin/streptomycin (17602E, Lonza, Basel, Switzerland), 0.1 μM PGE2 (Pfizer, New York, NY, USA), and 10 ng/mL murine GM-CSF (315-03, PeproTech, Rocky Hill, NJ, USA). After 3 days, mononuclear cells were cultured in osteoclast induction media, and BM-MIM supplemented with 10 ng/mL of receptor activator of NF-κB ligand (RANKL; 310-01, PeproTech) for another 7 days, changing the medium daily. Experiments were performed at least three times from two bone marrow extractions. Differentiations were done in duplicate or triplicate and conditioned medium for zymographic assay pooled from the replicas.

Gelatine zymography assay

The presence of MMPs with gelatinase activity in mouse cells was visualized by gelatin zymography assay. Ten to 20 μg of total protein from cell homogenates or equal volumes of culture conditioned media were mixed with nonreducing sample buffer (62.5 mM Tris-HCl, pH 6.8; 10% glycerol; 0.1% bromophenol blue). Electrophoresis was realized directly on 9% SDS-polyacrylamide gels (SDS-PAGE) containing 0.1% gelatin (w/v). After electrophoresis, gels were washed four times for 20 minutes at room temperature in a 2.5% (v/v) Triton X-100 solution to remove excess of SDS. Gels were transferred to zymogram development buffer solution (1610766, Bio-Rad Laboratories, Hercules, CA, USA) and incubated for at least 18 hours at 37°C.

Protein fixation was developed by incubating gels for 15 minutes with 50% methanol/7% acetic acid. Gels were then washed 30 minutes (six times of 5 minutes each) with distilled water. Lastly, gels were stained for 1 hour with GelCode Blue Stain Reagent (24590, Thermo Fisher Scientific) counterstained with distilled water and scanned.

Noncompetitive bone marrow transplantation

To create chimeras by noncompetitive bone marrow (BM) transplantation, 15 million whole-BM cells from donor mice ($n = 2$) were transplanted into lethally irradiated recipient mice (8 Gy from a cesium source 4 to 24 hours before transplantation). Chimeras were created by transplanting $Mmp10^{KO}$ mice (C57BL6/J background, CD45.2) and WT mice (C57BL6/J, CD45.2) with wild-type B6.SJL-derived BM (CD45.1). Cells were infused via lateral tail vein injection. Engraftment was monitored 10 weeks after transplantation by flow cytometry as previously described.[25] Data were analyzed using FlowJo Software (Becton, Dickinson and Company, Ashland, OR, USA).

Biomechanical testing

Mechanical tests were performed using a universal testing machine (Instron Mini44, Instron, Norwood, MA, USA) with a ± 500 N static load cell. For fixing testing samples to the machine, aluminum prisms, measuring 10 × 10 × 40 mm, were machined. The fixation method used for these experiments did not introduce any mechanical stress before testing. The detailed procedure for biomechanical testing is available in the Supplemental Materials and Methods.

Statistical analysis

Results are expressed as median with interquartile range and whiskers representing minimum and maximum values. Statistical analysis was performed using GraphPad Prism 9.0 software (GraphPad Software Inc, La Jolla, CA, USA). Normal distribution of the data was analyzed using Kolmogorov–Smirnov test. Single comparisons were analyzed by unpaired Student's *t* test when data presented normal distribution or the nonparametric Mann–Whitney *U* test when normal distribution was not present. Significance was set at $p < 0.05$.

Results

Expression profile of MMP-10 during fracture healing

To determine the expression profile and tissue distribution of MMP-10 during fracture healing, we performed closed diaphyseal tibial fractures in C57BL/6 (WT) mice and assessed the levels of MMP-10 by immunofluorescence at different stages of the reparative and resorptive phases of the fracture healing process. At the start of the reparative phase, 5 dpf, when chondrogenesis was incipient, the levels of MMP-10 were low, being at the limit of detection (data not shown). By 7 and 10 dpf, when the formation of cartilage peaked, MMP-10 could be detected in mononuclear and multinucleated cells in areas of cartilage resorption and in the surface of trabecular bone (Supplemental Fig. S1*A*). The maximum level of MMP-10 was detected at 14 dpf when the resorption of cartilage was almost completed. Finally, at 21 dpf, we detected low levels of MMP-10 in the trabecular bone of the hard callus (Supplemental Fig. S1*A*, *B*).

Mmp10^{KO} mice present delayed fracture healing

Based in the expression profile of MMP-10 during fracture healing, we speculated that its role would be centered at the resorption of cartilage. To assess this hypothesis, we performed tibial fractures in *Mmp10*-deficient mice (Mmp10^{KO}) and age- and sex-matched WT mice. In Mmp10^{KO} mice, fracture healing

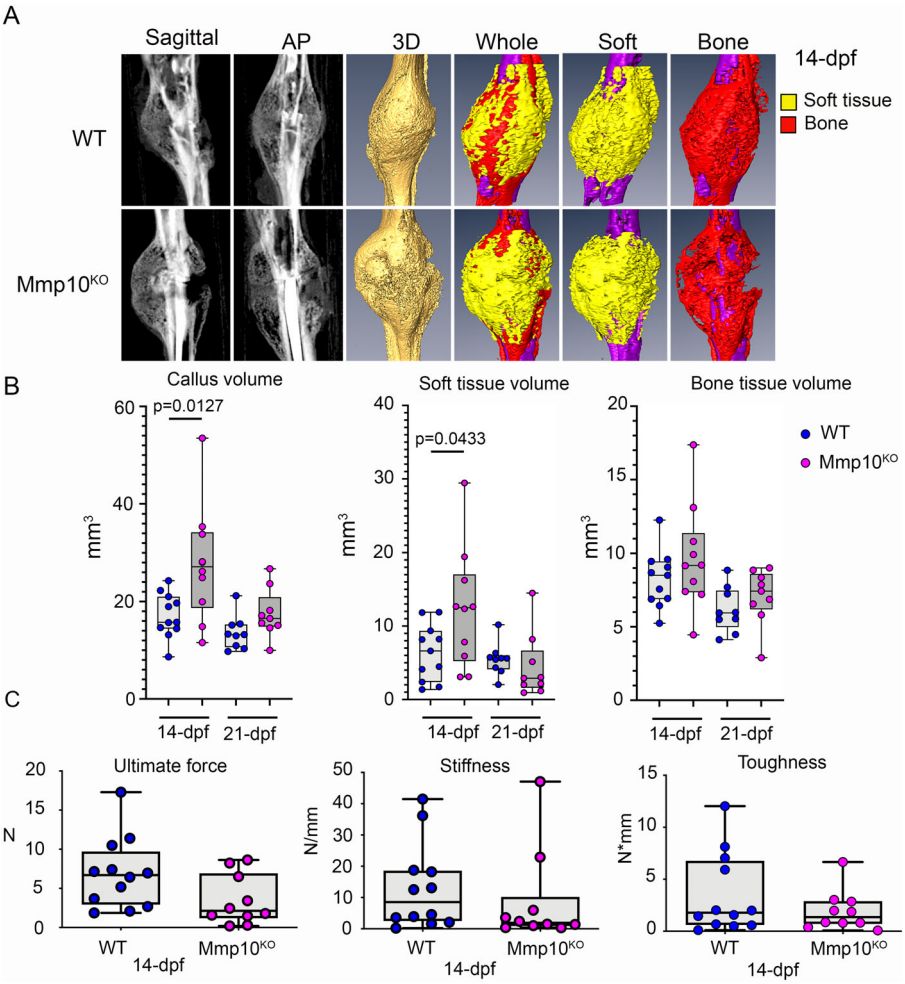

Fig 1. Micro-CT analysis and biomechanical properties of fracture calluses. (*A*) Representative radiographic planes, 3D reconstruction, and callus segmentation for WT and Mmp10^{KO} groups at 14 dpf. AP = coronal plane. (*B*) Quantification of total callus, bone, and soft tissue volumes at 14 (WT, $n = 11$; Mmp10^{KO}, $n = 9$) and 21 dpf (WT, $n = 10$; Mmp10^{KO}, $n = 9$). (*C*) Biomechanical test of fracture calluses at 14 dpf (WT, $n = 12$; Mmp10^{KO}, $n = 10$). Results are expressed as median with interquartile range, whiskers represent minimum and maximum values, and *p* values were determined by two-tailed Student's *t* test.

develops normally and a callus was evident at 14 dpf (Fig. 1*A*). However, at 14 dpf, the composition of the callus was altered in Mmp10^{KO} mice as detected by μCT, with a significant increase in the volume of the fracture callus because of an increase in nonmineralized tissue, with minor variations in the volume of the bone component (Fig. 1*B*). Nevertheless, this phenotype was transient, and at 21 dpf, the volumes of mineralized and nonmineralized tissue were similar at the fracture callus of Mmp10^{KO} and WT animals (Fig. 1*B* and Supplemental Fig. S2). The accumulation of soft tissue did not change the mechanical properties of the callus at 14 dpf as detected by biomechanical testing (ultimate force, $p = 0.0561$; stiffness, $p = 0.1985$; toughness, $p = 0.5310$) (Fig. 1*C*).

Increased cartilage tissue in fractured calluses of Mmp10^{KO} mice

To determine the nature of the accumulated soft tissue in Mmp10^{KO} mice, a histological analysis for the presence of cartilaginous tissue (GAG content) was performed during different phases of the fracture repair by TB. We found that WT and Mmp10^{KO} animals presented similar levels of cartilaginous tissue at 7 and 10 dpf. However, while by 14 dpf the TB staining was almost absent in WT animals, Mmp10^{KO} animals presented significant differences in cartilage tissue content (Fig. 2*A*, *B*).

Delayed cartilage remodeling in Mmp10^{KO} mice

To determine if the accumulation of cartilage tissue was the consequence from a delay in collagen production or from a reduction in cartilage resorption, we performed immunohistological analysis of the major cartilage components, type II and type X collagen. We found no differences in the levels of any of the collagens before 14 dpf and an accumulation of both collagens at this time point (Supplemental Fig. S3*A*, *B*), suggesting that the accumulation of cartilage was due to the defective resorption of the cartilaginous tissue. To confirm that the accumulation of cartilage was derived from a reduced resorption, we performed TRAP staining at different time points of the fracture healing process and quantified the presence of osteoclasts and related cells, TRAP^{+} cells, starting at 7 dpf. Mmp10^{KO} mice showed an increase in the number of TRAP^{+} in the fracture callus at 14 dpf (Fig. 3*A*). As expected, the accumulation was localized in the cartilage areas (Fig. 3*B*).

Normal intramembranous ossification mediated repair in Mmp10^{KO} mice

Because we detected increased number of TRAP^{+} cells in the cartilage of the fracture callus of Mmp10^{KO} mice, we ask if bone repair mediated by intramembranous ossification would be affected by the absence of MMP-10 activity. Performing a unicortical defect of the femur allowed us to induce bone damage that

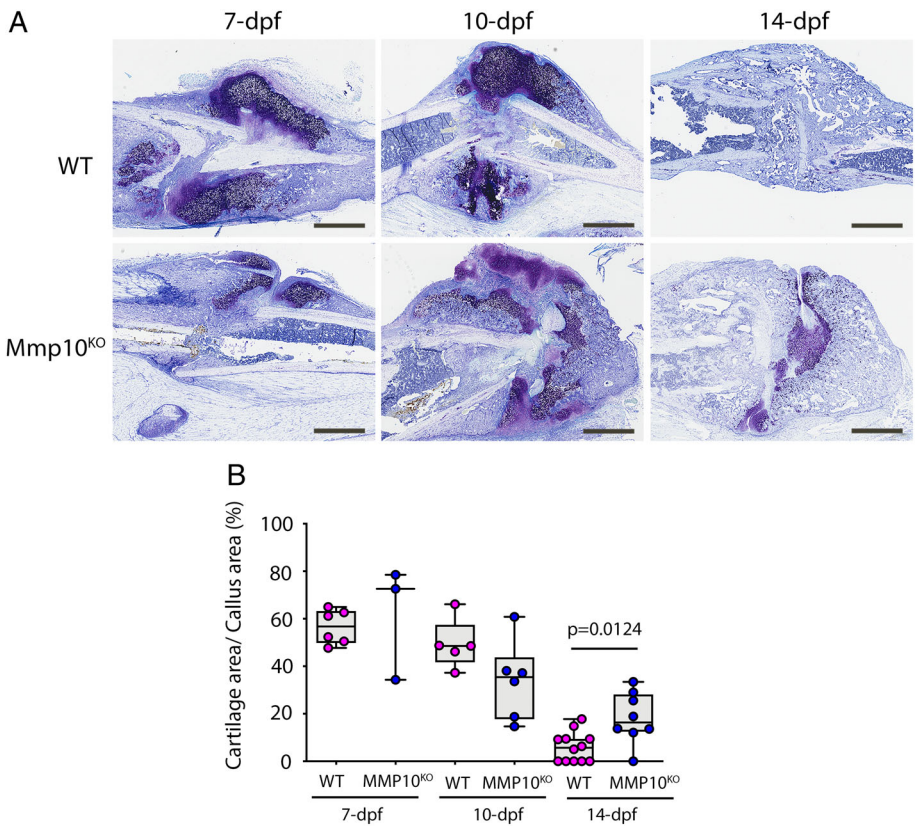

Fig 2. Histological and histomorphometric analysis of the fractured healing process in Mmp10^{KO} mice. (*A*) Toluidine blue staining of sagittal sections from WT and Mmp10^{KO} calluses. Scale bar = 1 mm. (*B*) Quantification of cartilage ratio in fracture calluses at 7 (WT, $n = 6$; Mmp10^{KO}, $n = 3$), 10 (WT, $n = 5$; Mmp10^{KO}, $n = 6$), and 14 dpf (WT, $n = 12$; Mmp10^{KO}, $n = 8$). Results are expressed as median with interquartile range, whiskers represent minimum and maximum values, and p value was determined by Mann–Whitney test.

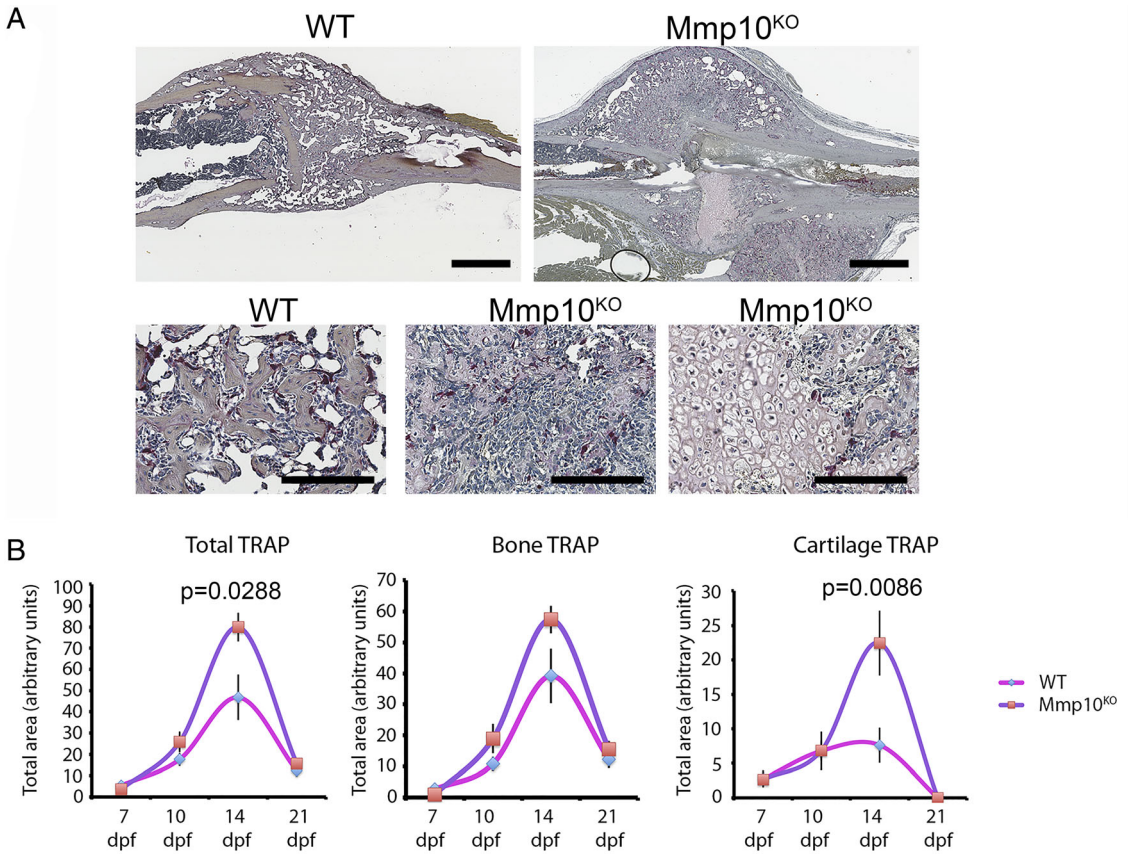

Fig 3. Analysis of the presence of osteoclasts in fractured calluses. (*A*) Representative TRAP staining in sagittal sections through the WT and Mmp10^{KO} calluses at 14 dpf. Scale bar = 1 mm (upper panels); 200 μm (bottom panels). (*B*) Quantification of TRAP-positive area in fracture calluses at 7 (WT, $n = 5$; Mmp10^{KO}, $n = 5$), 10 (WT, $n = 8$; Mmp10^{KO}, $n = 5$), 14 (WT, $n = 11$; Mmp10^{KO}, $n = 8$), and 21 dpf (WT, $n = 10$; Mmp10^{KO}, $n = 9$). Results are expressed as the median with interquartile range, whiskers represent minimum and maximum values, and *p* values were determined by two-tailed Student's *t* test.

presents mechanical stability initiating repair without formation of a cartilage intermediate. Radiographic analysis showed no gross differences in the repair of unicortical fractures between WT and Mmp10^{KO} mice (Supplemental Fig. S4*A*). At 14 dpf, quantification of bone content by μCT analysis showed an increase in new bone in Mmp10^{KO} mice; however, the increase does not reach statistical significance (Supplemental Fig. S4*B*). Finally, at 21 dpf, there were no major differences in the content of bone between Mmp10^{KO} and WT mice (Supplemental Fig. S4*B*, *C*).

Hematopoietic progenitors transplant rescues the phenotype of Mmp10^{KO} mice

To confirm that the phenotype observed is dependent on the activity of MMP-10 in TRAP^{+} cells, we designed a rescue experiment where the hematopoietic system of Mmp10^{KO} and WT mice (both CD45.2) was ablated by lethal γ irradiation and substituted by wild-type CD45.1 bone marrow-derived progenitor cells. In both types of animals, WT^{WT} and Mmp10^{WT}, CD45.1 progenitors engrafted, giving rise to similar content on cells of the myeloid lineage (Supplemental Fig. S5). Indeed, when subjected to a stabilized tibia fracture, 14-dpf radiographic appearance of the callus of Mmp10^{WT} and WT^{WT} animals was similar (Fig. 4*A*), and the volume and soft tissue composition of the callus was similar between groups with a slight increase in bone volume in Mmp10^{WT} (Fig. 4*B*). Histological analysis by TB staining confirmed similar levels of cartilage tissue between WT^{WT} and Mmp10^{WT} animals (Supplemental Fig. S5*B*).

Impaired processing of proMMP-9 in Mmp10^{KO} mice

To determine if the lack of MMP-10 activity has an effect over other MMPs, we differentiated in vitro bone marrow mononuclear cells derived from Mmp10^{KO} and WT mice into osteoclasts and determined the presence of MMPs with gelatinase activity by zymogram. Silencing *Mmp10* did not affect the differentiation process of mononuclear cells to osteoclasts, and similar number of TRAP-positive cells were observed in differentiated cultures of Mmp10^{KO} and WT-derived cells (data not shown). Zymogram of the cellular content of mononuclear cells and in vitro differentiated osteoclasts showed a single band with major gelatinase activity only in the in vitro differentiated osteoclasts, while no gelatinase activity was detected in cell lysates of mononuclear cells derived of Mmp10^{KO} or WT mice (Fig. 5*A*). The gelatinase activity present in the lysates showed reduced electrophoretic mobility, which was compatible with proMMP-9 when compared with recombinant active human MMP-9 or mouse eye tissue homogenate (Supplemental Fig. S6*A*).[26] Nevertheless, zymographic analysis of conditioned media showed that all cell populations derived from Mmp10^{KO}

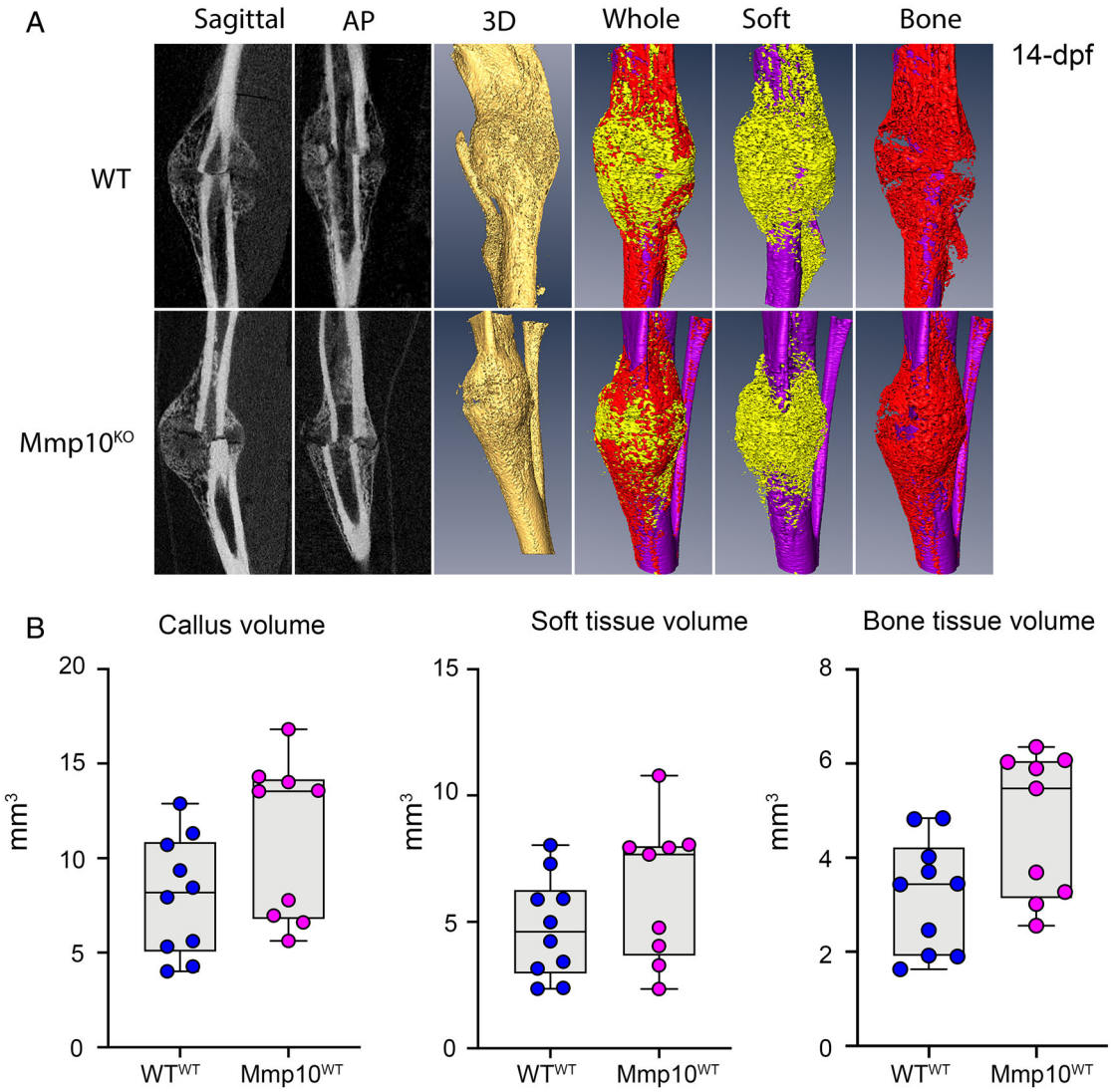

Fig 4. Mmp10^{KO} phenotype rescue by noncompetitive bone marrow transplantation. (*A*) Summary of the radiographic planes, 3D reconstruction, and callus segmentation for WT and Mmp10^{KO} transplanted mice fracture callus. (*B*) Comparison of callus, bone, and soft tissue volume at 14 dpf (WT^{WT}, $n = 10$; Mmp10^{WT}, $n = 9$). Results are expressed as the median with interquartile range, whiskers represent minimum and maximum values, and p values were determined by Mann–Whitney test.

and WT mice presented gelatinase activity, but only mononuclear cells derived from Mmp10^{KO} mice could not process proMMP-9 protein, and thus, lacking active lower molecular weight MMP-9 bands (Fig. 5*B*). Indeed, adding recombinant human MMP-10 to the conditioned media from Mmp10^{KO} results in processing of the proMMP-9 band and the appearance of lower molecular weight bands (Fig. 5*C*). Interestingly, in vitro differentiated osteoclasts from both Mmp10^{KO} and WT mice showed processed MMP-9 and an important increase of the gelatinase activity, indicating that in differentiated osteoclasts, other proteases can process proMMP-9 and suggesting that the lack of MMP-10 is important in mononuclear cells and the cause of the resulting phenotype.

To validate this hypothesis, we genetically labeled hematopoietic populations in vivo with ZsGreen fluorescence by pI:pC induction in Mx1-CreAi6 mice[27,28] and performed nonstabilized tibia fractures to enhance endochondral ossification. Ten days post-fracture, when cartilaginous content peaks in the fracture callus, we investigated the presence of MMP-9 and MMP-10 together with ZsGreen-labeled cells. ZsGreen^{+} cells were abundant in the edges of cartilage tissue, in newly synthesized bone as well as in fibrous tissue, and absent in cartilage. Some of these cells were F4/80^{+} that identifies macrophages (Fig. 5*D*). MMP-9 and MMP-10 were expressed in similar locations, while in the edges of cartilage tissue and in the areas of fibrous tissue, we detected low expression of the metalloproteases and a strong signal was detected in multinucleated cells, especially in newly synthesized bone areas (Supplemental Fig. S6*B*).

Discussion

In this report, we demonstrate that deleting *Mmp10* results in a delayed fracture healing phenotype characterized by the

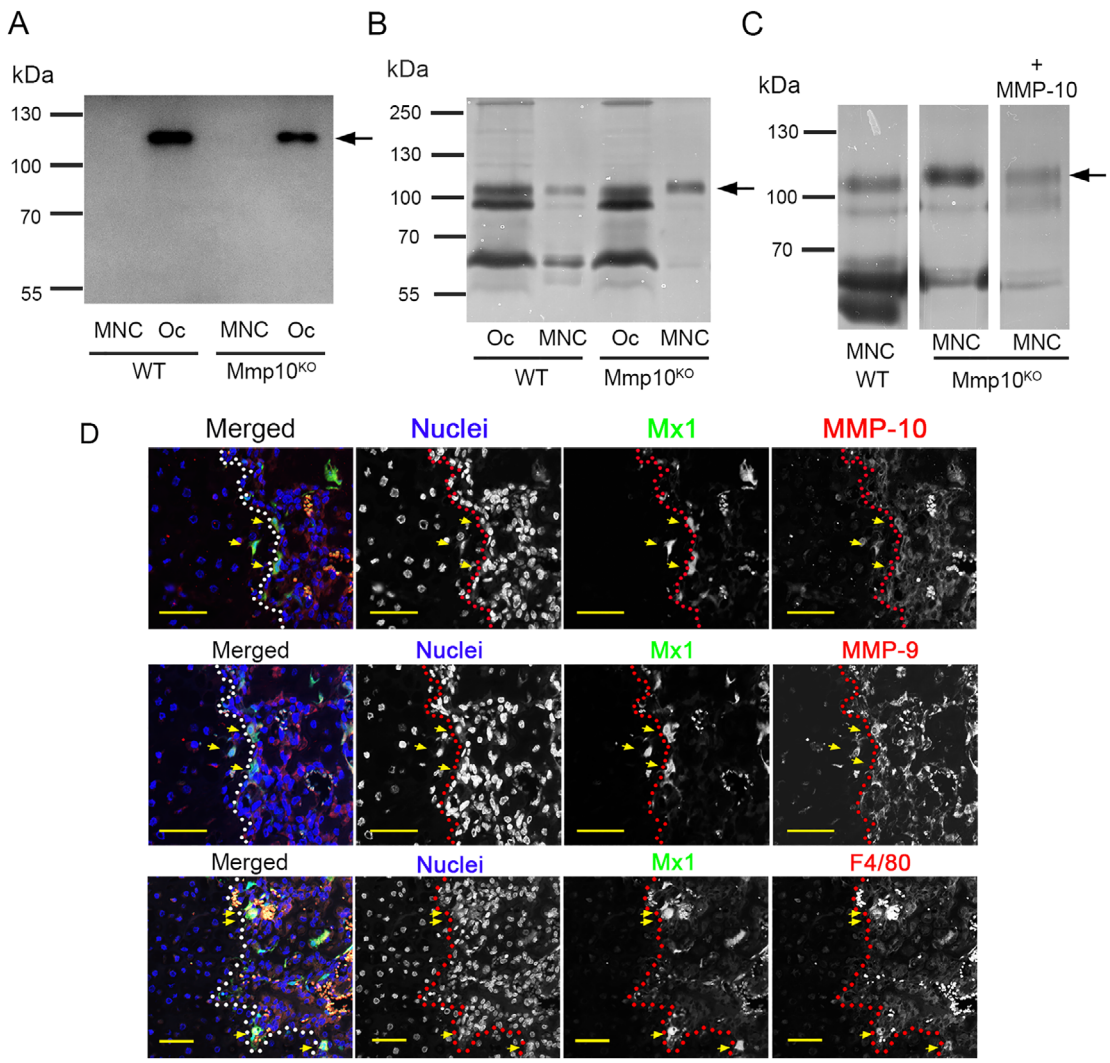

Fig 5. Reduced gelatinase activity in Mmp10^{KO} mice. (*A*) Gelatinase activity in lysates of bone marrow mononuclear cells (MNC) and MNC differentiated in vitro to osteoclasts (Oc), visualized by in gel zymographic assay. (*B*) The gelatinase activity detected in the cell lysates of differentiated osteoclasts was compatible with proMMP-9 activity. CM = conditionate medium. (*C*) Presence of gelatinase activity in CM from MNC and in vitro differentiated osteoclasts. (*D*) Detection of cells of hematopoietic lineage (Mx1^{+}, green) at the edge of the cartilage (doted lines) at 10 dpf. Scale bar = 50 μm.

accumulation of cartilaginous tissue. This phenotype is transient and could be rescued by noncompetitive transplant of hematopoietic progenitors. The observed phenotype in *Mmp10* knockout mice correlates well with the expression pattern of MMP-10, being cells of hematopoietic origin, osteoclasts, and monocyte/macrophages, the major cell populations expressing MMP-10. In addition, we found that the silencing of *Mmp10* results in impaired proMMP-9 processing that suggests MMP-10 as a major in vivo activator of proMMP-9 in murine monocytes/macrophages. Taken together, our results suggest that monocytes/macrophages participate in the early steps of cartilaginous callus vascularization, priming ECM degradation, and that MMP-10/MMP-9 have a leading role in this process (Fig. 6*A*, *B*).

During the formation of the skeleton and in the progression of fracture healing by endochondral ossification, a critical step is the vascularization and remodeling of the cartilaginous extracellular matrix.[6,29,30] In these processes, MMPs have a central role, due to the variety of substrates that they can recognize. Among all MMPs, only a few have been evaluated in the fracture healing process, having collagenases and gelatinases the leading role in cartilage removal and callus vascularization.[8-10] In fracture healing, it is well stablished that silencing *Mmp9* or *Mmp13* results in similar phenotypes, characterized by an accumulation of cartilage and impaired revascularization of the callus, although *Mmp9* is expressed primarily in macrophages/osteoclasts, while *Mmp13* is expressed in hypertrophic chondrocytes and osteoblasts.[9,10] It also has been suggested that because of the synergy between MMP-9 and MMP-13 to degrade cartilaginous tissue, MMP-13 from hypertrophic chondrocytes would cleave different collagen types (type II, type X, and type I between others), while MMP-9 from macrophages and osteoclasts would clear the denatured cartilage resulting from MMP-13 activity. The phenotype observed in double mutant mice (Mmp13$^{-/-}$/Mmp9$^{-/-}$), characterized by severely impaired endochondral

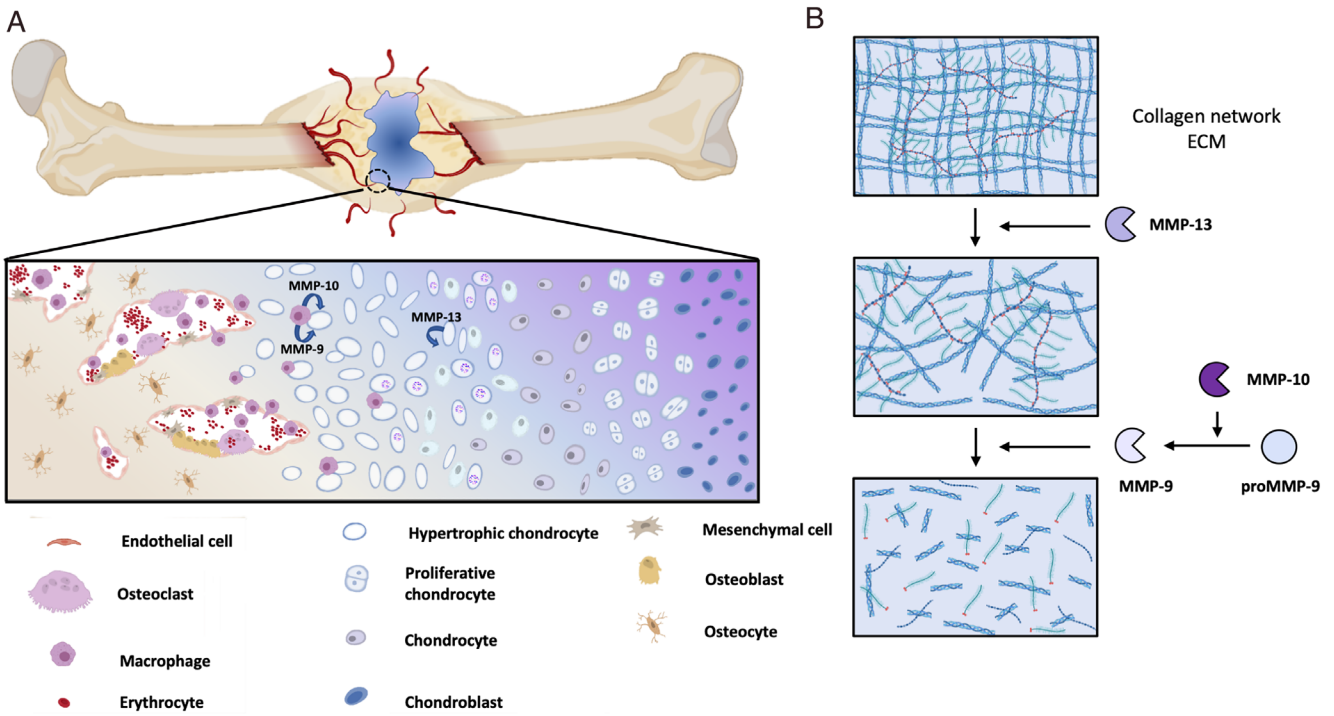

Fig 6. MMP-10 function during endochondral fracture healing. Cellular (*A*) and molecular mechanisms (*B*) of MMP-10 in fracture healing. Hypertrophic chondrocytes secrete MMP-13 for the processing of native collagen network. Monocyte/macrophages secrete proMMP-9 and MMP-10 for further processing of the partially cleaved collagen, priming vascular invasion.

bone, delayed vascular recruitment, and defective trabecular bone formation, supports this hypothesis.[31] On the other hand, silencing *Mmp2* results in delayed bone phenotype that courses without impaired cartilage remodeling.[8] Therefore, while the observed phenotype, osteoclast accumulation and delayed cartilage resorption, recapitulates that of both $Mmp9^{KO}$ and $Mmp13^{KO}$ phenotypes, the expression pattern is more related to the phenotype observed for the lack of the gelatinase MMP-9 than the phenotype reported for the lack of the collagenase MMP-13. In addition, *Mmp10* and *Mmp9* knockout phenotypes can be rescued by a noncompetitive bone marrow transplantation, while *Mmp13* knockout associated phenotype cannot.[9,10,32]

MMP-9 has been defined as a key element for the vascularization of the growth plate and in the revascularization of ischemic tissue. MMP-9 expressed by macrophages is needed for correct branching.[33,34] MMP-9 is secreted as zymogen requiring for its activation proteolytic processing of the regulatory pro-domain. This processing has been evaluated in vitro with a number of proteinases, plasmin, cathepsin G and K, and metalloproteinases, including MMP-2, MMP-7, MMP-13, as well as MMP-3 and MMP-10, showing specificity for this processing.[35-42] MMP-3 has been proposed as the protease that functions as the activator of MMP-9 in vivo, however inferred from in vitro evidence.[39,43] Recently, proMMP-9 has been identified as a substrate for MMP-10 in the skin using in vivo degradomics and confirmed by analysis of the secretome of keratinocytes.[44] Here, we provide compelling evidence of in vivo activation of MMP-9 by MMP-10 and its implication in fracture healing.

Macrophages have been implicated in all phases of fracture healing and depletion of macrophages in murine models of fracture healing demonstrate their indispensable function in the later phase of fracture healing.[45-47] We found that monocytes/macrophages expressing MMP-10 participate in fracture healing and that they localize at the edges of cartilage tissue, priming cartilaginous callus remodeling and vascular invasion. This specific location for macrophages has also been reported elsewhere in endochondral ossification, both in fracture repair as well as in the formation of the secondary ossification center. Interestingly, in the latest, MT1-MMP is the protease leading the process and its ablation results in deficient vascularization and delayed secondary ossification center formation.[45,48,49]

In conclusion, during fracture healing, MMP-10 activity is expressed in cells of hematopoietic origin. Its activity is needed in monocytes/macrophages for the processing of proMMP-9 and further remodeling of the cartilaginous callus for the progression of the healing process.

Disclosures

All authors state that they have no conflicts of interest.

Acknowledgments

This work was supported by funds from Mineco (Ministerio de Asuntos Económicos y Transformación Digital) through Instituto de Salud Carlos III and European Regional Development Funds (PI20/00076 and PI17/00136 to FG-M and ISCIII-RETICS RD16/0011/0005 to FP), European Union Horizon 2020 program (874889, HEALIKICK to FG-M), and Departamento de Desarrollo Económico del Gobierno de Navarra (PC009-010-011 3DMedical

and PC073-074-075 3DMedical to FG-M). JV-F and JR-T are supported by a fellowship of the Asociación de Amigos de la Universidad de Navarra. We want to express our gratitude to the Experimental Ophthalmology Laboratory, Clínica Universidad de Navarra, for zymographic assays advice and discussion.

Authors' roles: Study design: JAR, JAP, JO, FP, and FG-M. Data collection: JV-F, TL-M, PR-C, IC, BS, JR-T, JA, EM-L, and VM. Data interpretation: FP and FG-M. Drafting manuscript: JV-F and FG-M. All authors revised content and approved the final version of the manuscript and the integrity of the data.

PEER REVIEW

The peer review history for this article is available at https://publons.com/publon/10.1002/jbmr.4403.

DATA AVAILABILITY STATEMENT

The data that support the findings of this study are available from the corresponding author upon reasonable request.

References

1. Schindeler A, McDonald MM, Bokko P, Little DG. Bone remodeling during fracture repair: the cellular picture. Semin Cell Dev Biol. 2008;19(5):459-466.
2. Runyan CM, Gabrick KS. Biology of bone formation, fracture healing, and distraction osteogenesis. J Craniofac Surg. 2017;28(5):1380-1389.
3. Graves DT, Alagl AS, Einhorn TA, ZS AI-A, Gerstenfeld LC. Molecular mechanisms controlling bone formation during fracture healing and distraction osteogenesis. J Dent Res. 2009;87(2):107-118.
4. Aiken A, Khokha R. Unraveling metalloproteinase function in skeletal biology and disease using genetically altered mice. Biochim Biophys Acta Mol Cell Res. 2010;1803(1):121-132.
5. Stamenkovic I. Extracellular matrix remodelling: the role of matrix metalloproteinases. J Pathol. 2003;200(4):448-464.
6. Ortega N, Behonick DJ, Werb Z. Matrix remodeling during endochondral ossification. Trends Cell Biol. 2004;14(2):86-93.
7. Paiva KBS, Granjeiro JM. Bone tissue remodeling and development: focus on matrix metalloproteinase functions. Arch Biochem Biophys. 2014;561:74-87.
8. Behonick D, Lieu S, Hansen E, et al. Impaired remodeling phase of fracture repair in the absence of matrix metalloproteinase-2. Dis Model Mech. 2010;4(2):203-211.
9. Colnot C, Thompson Z, Miclau T, Werb Z, Helms JA. Altered fracture repair in the absence of MMP9. Development. 2003;130(17):4123-4133.
10. Kosaki N, Takaishi H, Kamekura S, et al. Impaired bone fracture healing in matrix metalloproteinase-13 deficient mice. Biochem Biophys Res Commun. 2007;354(4):846-851.
11. Uusitalo H, Hiltunen A, Söderström M, Aro HT, Vuorio E. Expression of cathepsins B, H, K, L, and S and matrix metalloproteinases 9 and 13 during chondrocyte hypertrophy and endochondral ossification in mouse fracture callus. Calcif Tissue Int. 2000;67(5):382-390.
12. Madlener M, Werner S. cDNA cloning and expression of the gene encoding murine stromelysin-2 (MMP-10). Gene. 1997;202(1–2):75-81.
13. Orbe J, Barrenetxe J, Rodriguez JA, et al. Matrix metalloproteinase-10 effectively reduces infarct size in experimental stroke by enhancing fibrinolysis via a thrombin-activatable fibrinolysis inhibitor–mediated mechanism. Circulation. 2011;124(25):2909-2919.
14. Gill JH, Kirwan IG, Seargent JM, et al. MMP-10 is overexpressed, proteolytically active, and a potential target for therapeutic intervention in human lung carcinomas. Neoplasia. 2004;6(6):777-785.
15. Garcia-Irigoyen O, Carotti S, Latasa MU, et al. Matrix metalloproteinase-10 expression is induced during hepatic injury and plays a fundamental role in liver tissue repair. Liver Int. 2014;34(7):e257-e270.
16. Bord S, Horner A, Hembry RM, Compston JE. Stromelysin-1 (MMP-3) and stromelysin-2 (MMP-10) expression in developing human bone: potential roles in skeletal development. Bone. 1998;23(1):7-12.
17. Mao L, Yano M, Kawao N, Tamura Y, Okada K, Kaji H. Role of matrix metalloproteinase-10 in the BMP-2 inducing osteoblastic differentiation. Endocr J. 2013;60(12):1309-1319.
18. Birkland TP, Rowan AD, Howe JD, et al. Macrophage migration and invasion is regulated by MMP10 expression. PLoS One. 2013;8(5):e63555.
19. McMahan RS, Birkland TP, Smigiel KS, et al. Stromelysin-2 (MMP10) moderates inflammation by controlling macrophage activation. J Immunol. 2016;197(3):899-909.
20. Kassim SY, Gharib SA, Mecham BH, Birkland TP, Parks WC, JK MG. Individual matrix metalloproteinases control distinct transcriptional responses in airway epithelial cells infected with *Pseudomonas aeruginosa*. Infect Immun. 2007;75(12):5640.
21. Muinos-López E, Ripalda-Cemboráin P, López-Martínez T, et al. Hypoxia and reactive oxygen species homeostasis in mesenchymal progenitor cells define a molecular mechanism for fracture nonunion. Stem Cells. 2016;34(9):2342-2353.
22. Granero-Moltó F, Weis JA, Miga MI, et al. Regenerative effects of transplanted mesenchymal stem cells in fracture healing. Stem Cells. 2009;27(8):1887-1898.
23. González-Gil AB, Lamo-Espinosa JM, Muiños-López E, et al. Periosteum-derived mesenchymal progenitor cells in engineered implants promote fracture healing in a critical-size defect rat model. J Tissue Eng Regen Med. 2019;13(5):742-752.
24. Tevlin R, McArdle A, Chan CKF, et al. Osteoclast derivation from mouse bone marrow. J Vis Exp. 2014;93:e52056.
25. Saez B, Ferraro F, Yusuf RZ, et al. Inhibiting stromal cell heparan sulfate synthesis improves stem cell mobilization and enables engraftment without cytotoxic conditioning. Blood. 2014;124(19):2937-2947.
26. De Groef L, Andries L, Lemmens K, Van Hove I, Moons L. Matrix metalloproteinases in the mouse retina: a comparative study of expression patterns and MMP antibodies retina. BMC Ophthalmol. 2015;15:187.
27. Kuhn R, Schwenk F, Aguet M, Rajewsky K. Inducible gene targeting in mice. Science. 1995;269(5229):1427-1429.
28. Yang S, Li Y-P, Liu T, et al. Mx1-cre mediated Rgs12 conditional knockout mice exhibit increased bone mass phenotype. Genesis. 2013;51(3):201-209.
29. Einhorn TA, Gerstenfeld LC. Fracture healing: mechanisms and interventions. Nat Rev Rheumatol. 2015;11(1):45-54.
30. Hausman MR, Schaffler MB, Majeska RJ. Prevention of fracture healing in rats by an inhibitor of angiogenesis. Bone. 2001;29(6):560-564.
31. Stickens D, Behonick DJ, Ortega N, et al. Altered endochondral bone development in matrix metalloproteinase 13-deficient mice. Development. 2004;131(23):5883-5895.
32. Behonick DJ, Xing Z, Lieu S, et al. Role of matrix metalloproteinase 13 in both endochondral and intramembranous ossification during skeletal regeneration. PLoS One. 2007;2(11):e1150. .
33. Vu TH, Shipley JM, Bergers G, et al. MMP-9/gelatinase B is a key regulator of growth plate angiogenesis and apoptosis of hypertrophic chondrocytes. Cell. 1998;93(3):411-422.
34. Johnson C, Sung H-J, Lessner SM, Fini ME, Galis ZS. Matrix metalloproteinase-9 is required for adequate angiogenic revascularization of ischemic tissues. Circ Res. 2004;94(2):262-268.
35. Davis GE, Pintar Allen KA, Salazar R, Maxwell SA. Matrix metalloproteinase-1 and -9 activation by plasmin regulates a novel endothelial cell-mediated mechanism of collagen gel contraction and capillary tube regression in three-dimensional collagen matrices. J Cell Sci. 2001;114(Pt 5):917-930.
36. Wilson TJ, Nannuru KC, Singh RK. Cathepsin G-mediated activation of pro-matrix metalloproteinase 9 at the tumor-bone interface promotes transforming growth factor-signaling and bone destruction. Mol. Cancer Res. 2009;7(8):1224-1233.

37. Christensen J, Shastri VP. Matrix-metalloproteinase-9 is cleaved and activated by Cathepsin K. BMC Res Notes. 2015;8(1):322.

38. Fridman R, Toth M, Peña D, Mobashery S. Activation of progelatinase B (MMP-9) by gelatinase A (MMP-2). Cancer Res. 1995;55(12):2548-2555.

39. Ogata Y, Enghild JJ, Nagase H. Matrix metalloproteinase 3 (stromelysin) activates the precursor for the human matrix metalloproteinase 9. J Biol Chem. 1992;267(6):3581-3584.

40. Imai K, Yokohama Y, Nakanishi I, et al. Matrix metalloproteinase 7 (matrilysin) from human rectal carcinoma cells. Activation of the precursor, interaction with other matrix metalloproteinases and enzymic properties. J Biol Chem. 1995;270(12):6691-6697.

41. Nakamura H, Fujii Y, Ohuchi E, Yamamoto E, Okada Y. Activation of the precursor of human stromelysin 2 and its interactions with other matrix metalloproteinases. Eur J Biochem. 1998;253(1):67-75.

42. Knauper V, Smith B, Lopez-Otin C, Murphy G. Activation of progelatinase B (proMMP-9) by active collagenase-3 (MMP-13). Eur J Biochem. 1997;248(2):369-373.

43. Shapiro SD, Fliszar CJ, Broekelmann TJ, Mecham RP, Senior RM, Welgus HG. Activation of the 92-kDa gelatinase by stromelysin and 4-aminophenylmercuric acetate. J Biol Chem. 1995;270(11):6351-6356.

44. Schlage P, Kockmann T, Sabino F, Kizhakkedathu JN, Auf dem Keller U. Matrix metalloproteinase 10 degradomics in keratinocytes and epidermal tissue identifies bioactive substrates with pleiotropic functions. Mol Cell Proteomics. 2015;14(12):3234-3246.

45. Raggatt LJ, Wullschleger ME, Alexander KA, et al. Fracture healing via periosteal callus formation requires macrophages for both initiation and progression of early endochondral ossification. Am J Pathol. 2014;184(12):3192-3204.

46. Schlundt C, El Khassawna T, Serra A, et al. Macrophages in bone fracture healing: their essential role in endochondral ossification. Bone. 2018;106:78-89.

47. Lin H-N, O'Connor JP. Osteoclast depletion with clodronate liposomes delays fracture healing in mice. J Orthop Res. 2017;35(8):1699-1706.

48. Blumer MJF, Longato S, Fritsch H. Localization of tartrate-resistant acid phosphatase (TRAP), membrane type-1 matrix metalloproteinases (MT1-MMP) and macrophages during early endochondral bone formation. J Anat. 2008;213(4):431-441.

49. Zhou Z, Apte SS, Soininen R, et al. Impaired endochondral ossification and angiogenesis in mice deficient in membrane-type matrix metalloproteinase I. Proc Natl Acad Sci U S A. 2000;97(8):4052-4057.